J Assist Reprod Genet (2016) 33:1041–1057
DOI 10.1007/s10815-016-0739-8

GAMETE BIOLOGY

Ultrastructural and cytogenetic analyses of mature human oocyte dysmorphisms with respect to clinical outcomes

Mário Sousa[1,2] · Mariana Cunha[3] · Joaquina Silva[3] · Elsa Oliveira[1,2] · Maria João Pinho[4,5] · Carolina Almeida[4,5] · Rosália Sá[1,2] · José Teixeira da Silva[3] · Cristiano Oliveira[3] · Alberto Barros[3,4,5]

Received: 26 February 2016 / Accepted: 13 May 2016 / Published online: 24 May 2016

Abstract
Purpose The study aimed to describe the ultrastructure of two human mature oocyte intracytoplasmic dysmorphisms, the bull-eye inclusion and the granular vacuole, with evaluation of clinical outcomes after intracytoplasmic sperm injection (ICSI) treatment.
Methods We retrospectively evaluated 4099 consecutive ICSI cycles during the period 2003–2013. Three groups were compared: controls, those with a bulls-eye inclusion, and those with granular vacuoles. Oocyte dysmorphisms were evaluated by transmission electron microscopy and in situ fluorescence hybridization (FISH). Detailed data on demographic and stimulation characteristics, as well as on embryological, clinical, and newborn outcomes, are fully presented.
Results The bull-eye inclusion is a prominent smooth round structure containing trapped vesicles, being surrounded by lipid droplets. The presence of this dysmorphism in the oocyte cohort had no clinical impact except when transferred embryos were exclusively derived from dysmorphism oocytes. The granular vacuole is delimited by a discontinuous double membrane and contains lipid droplets and vesicles. As FISH analysis revealed the presence of chromosomes, they probably represent pyknotic nuclei. The presence of this dysmorphism in the oocyte cohort had no clinical impact except when at least one transferred embryo was derived from dimorphic oocytes.
Conclusions Poor clinical outcomes were observed with transfer of embryos derived from dysmorphism oocytes, although without causing gestation or newborn problems. The bull-eye inclusion and granular vacuoles may thus be new prognostic factors for clinical outcomes.

Keywords Oocyte dysmorphisms · Bull-eye inclusion · Granular vacuoles · Ultrastructure · Oocyte cytogenetics · Clinical outcomes

Capsule Poor clinical outcomes were observed with mixed or pure transfer of embryos derived from oocytes containing bull-eye inclusions or granular-vacuoles. These dimorphisms may be new prognostic factors for clinical outcomes.

Electronic supplementary material The online version of this article (doi:10.1007/s10815-016-0739-8) contains supplementary material, which is available to authorized users.

✉ Mário Sousa
msousa@icbas.up.pt

[1] Department of Microscopy, Laboratory of Cell Biology, Institute of Biomedical Sciences Abel Salazar (ICBAS), University of Porto (UP), Rua Jorge Viterbo Ferreira, 228, 4050-313 Porto, Portugal

[2] Multidisciplinary Unit for Biomedical Research-UMIB, ICBAS-UP, Rua Jorge Viterbo Ferreira, 228, 4050-313 Porto, Portugal

[3] Centre for Reproductive Genetics Alberto Barros (CGR), Av. do Bessa, 240, 1° Dto. Frente, 4100-009 Porto, Portugal

[4] Department of Genetics, Faculty of Medicine, University of Porto, Alameda Prof. Hernâni Monteiro, 4200-319 Porto, Portugal

[5] Institute of Health Research an Innovation (I3S), UP, Alameda Prof. Hernâni Monteiro, 4200-319 Porto, Portugal

Introduction

A large proportion of human mature (MII) oocytes retrieved after controlled ovarian hyperstimulation displays extracytoplasmic (zona pellucida, polar body, perivitelline space) or intracytoplasmic dysmorphisms [1, 2]. The latter have been reported to occur in about 10–15 % of human MII oocytes, with an associated aneuploidy rate of 20–65 % [1, 3].

The success of assisted reproductive treatments depends on the oocyte quality. A competent oocyte requests full

cytoplasmic and nuclear maturity [4–8]. Therefore, numerous factors have been referred as relevant for oocyte competence such as zona pellucida (ZP) morphology [9–12]; polar body morphology, and chromosome constitution [13–18]; metaphase spindle [19–21]; chromosome constitution [1, 2, 7, 22]; oocyte DNA damage and repair [22]; cytoplasmic viscosity and resistance to membrane penetration during intracytoplasmic sperm injection (ICSI) [7, 23, 24]; oocyte shape [7, 25, 26]; mitochondria aggregation patterns [27, 28]; diverse extracytoplasmic and intracytoplasmic inclusions [5–8]; and abnormal expressed genes [29–32].

The large majority of studies on oocyte cytoplasmic dimorphisms provided individual embryological information, although the individual impact of these dimorphisms remains unclear as most of the clinical results are presented for pooled oocyte dimorphisms [33–44].

Other authors, nevertheless, analyzed specific oocyte cytoplasmic dimorphisms after ICSI cycles providing thus more accurate information about the dimorphisms studied. Refractile bodies (RB) are a very common inclusion consisting on a secondary lysosome with incorporated autophagy materials. RB were associated with decreased fertilization rate (FR), embryo cleavage rate (ECR), and blastocyst development when >5 μm [45]. Oocytes with a central dark granulation are also frequent and correspond to an abnormal accumulation of mitochondria and vesicles. No significant differences were observed for the FR, ECR, embryo quality, or clinical pregnancy (CP) rate. On the contrary, it was observed that there were significant lower implantation (IR) and ongoing pregnancy (OP) rates and a higher embryo aneuploidy rate [29, 46, 47]. Vacuoles are large vesicles [1, 33, 34, 38], which have an estimated frequency of 3.9 % [48]. They have been related with the absorption of perivitelline space fluid [1] or with the dilation of smooth endoplasmic reticulum (SER) components [49–51], being thus considered morphological degenerative changes [49–51]. The FR was found decreased when multiple vacuoles or vacuoles >14 μm were present [48]. A case report on recurrent central very large vacuole reported the birth of a newborn (NB) with a major malformation (double left kidney and ureter) [52]. The smooth vacuole was described as a large aggregate of SER tubules surrounded by mitochondria (aSERT). This dimorphism was associated with lower embryo quality, IR, CP rate, and birth of a NB presenting a Beckwith-Wiedemann syndrome [53]. Another study found a decrease in the rate of blastocyst formation, a higher abortion rate, a lower live birth delivery rate (LBDR), higher preterm birth, decreased birth weight, higher rate of neonatal death, and a case presenting a diaphragmatic hernia [54]. In a case report with recurrent large aSERT, authors reported two OP, one interrupted by abortion due to holoproencephaly and other that resulted in a neonatal death due to multiple anomalies [55]. The most complete study on large aSERT showed that this has a frequency of 1.7 %. The authors observed a significant higher number of retrieved oocytes and immaturity rate, lower FR, ECR, blastocyst formation rate, IR, CP rate, OP rate and LBDR, higher preterm birth, and the birth of a NB with a small ventricular septal defect [56]. However, a similar work delivered opposite results, with all rates being similar to controls without NB malformations [57]. A recent report revealed lower FR and IR, without adverse effects on the other clinical and NB outcomes [58]. The actual evidence and guidelines suggest hence that transfer of embryos derived from oocytes with large aSERT should be avoided [59–61].

In the present study, we describe the ultrastructure of two human oocyte cytoplasmic dimorphisms, the bull-eye inclusion and the granular vacuole, along with the evaluation of clinical outcomes. Fluorescence in situ hybridization (FISH) analysis revealed the presence of chromosome material in granular vacuoles, thus suggesting that they probably represent pyknotic micronuclei. Poor clinical outcomes were observed after transfer of embryos derived from dimorphic oocytes, though there was no gestation or NB problems. The bull-eye inclusion and granular vacuoles may thus be new prognostic factors for clinical outcomes.

Material and methods

Ethics approval

According to the National Law on Medically Assisted Procreation (Law 32/2006) and the National Council on Medically Assisted Procreation guidelines (CNPMA, 2008), patient samples and data bases were used after patient's informed and written consent from cases enrolled in infertility treatments.

Patients

We retrospectively evaluated 4099 consecutive ICSI cycles with ejaculated sperm over the period 2003–2013. Three groups were analyzed: controls (3877 cycles), cases with a bull-eye inclusion in MII oocytes (11 cycles), and cases with a granular vacuole in MII oocytes (211 cycles).

Karyotype analysis

The karyotype was obtained using G-banding and included the analysis of at least 30 metaphases from peripheral blood lymphocytes, according to general protocols [62].

Stimulation protocol

Women underwent controlled ovarian hyperstimulation with a gonadotropin-releasing hormone (GnRH) short antagonist multiple-dose flexible protocol in the large majority of the cases (Cetrorelix: Merck Serono, Geneve, Switzerland;

Ganirelix: Organon, Oss, Netherlands) and the long agonist protocol (Busereline, Suprefact: Sanofi Aventis, Frankfurt, Germany) in the other cases [63, 64]. For stimulation, recombinant follicle-stimulating hormone (rFSH; IU/ml; Puregon: Organon; Gonal-F: Merck Serono) was used. In several cases, human menopausal gonadotropin (HMG; Menopur: Ferring, Kiel, Germany) was added to rFSH and in a few cases only HMG was used. About 36 h before oocyte recovery, human chorionic gonadotropin (hCG; 5000–10,000 IU, im/sc; Pregnyl: Organon) was administered. In cases at risk of ovarian hyperstimulation syndrome, Busereline was used instead of hCG. Estradiol serum levels were assayed at the day of hCG or 1 day before [63, 64].

Gamete and embryo handling

Media from Medicult (Jyllinge, Denmark) or Vitrolife (Kungsbacka, Sweden) were used for gamete and embryo handling. Microinjection was executed in an inverted microscope (Nikon DIAPHOT 200; Nikon, Tokyo, Japan), equipped with a thermal plate (37 °C), Hoffman optics (Nikon), and Narishige micromanipulators (MO-188; Narishige, Tokyo, Japan), using micropipettes from Swemed (Goteborg, Sweden). ICSI was performed using the strong dislocation of the cytoplasm [65]. Embryo quality was graded according to described methods [66, 67]. Embryo transfer was accomplished under ultrasonography, using a Sure View Wallace Embryo Replacement Catheter or Wallace malleable stylet (Smiths Medical International, Kent, UK).

Luteal supplementation

All patients had luteal supplementation with intravaginal administration of 200 mg of natural-micronized progesterone (Jaba, Besins International, Montrouge, France), 8/8 h (600 mg day) beginning on the day of oocyte retrieval. Implantation was confirmed by a rise in β-hCG serum 12 days after embryo transfer. Progesterone was maintained until β-hCG serum assay and, if positive, it was continued until 12 weeks of gestation. Clinical pregnancy was established by ultrasound visualization of a gestational sac at 7 weeks of gestation. Where a GnRH agonist was used for triggering final oocyte maturation, luteal support was associated with an oral tablet of 2 mg estradiol (Isdin, Novo Nordisk, Bagsvaerd, Denmark), 12/12 h for the same time of progesterone and hCG (1500 IU) at the day of oocyte pick-up [68].

Cell imaging, transmission electron microscopy, and fluorescence in situ hybridization

Live cell images were taken under the inverted microscope using the Cronus-3 imaging system (Research-Instruments Ltd, Cornwall, UK).

Immediately after denudation, 11 excedentary dimorphic MII oocytes were processed, 6 for transmission electron microscopy (TEM) and 5 for FISH. Normal MII oocytes from a dimorphic cohort were not processed for TEM as they were not donated for research. Nevertheless, a TEM image of a normal MII oocyte from our archives is presented for comparisons (Fig. 1g).

Four oocytes with a granular vacuole (two of small and two of medium size) and two oocytes with a bull-eye inclusion were fixed with Karnovsky (2.5 % glutaraldehyde, 4 % paraformaldehyde, 0.15 M sodium cacodylate buffer, pH 7.3) (Sigma-Aldrich, St. Louis, USA; Merck, Darmstadt, Germany) for 30 min at room temperature and then for 2 h at 4 °C, washed in buffer overnight at 4 °C, post-fixed in 2 % osmium tetraoxide (Merck) in buffer containing 0.8 % potassium ferricyanide (Merck) for 2 h at 4 °C, washed in buffer (10 min), serially dehydrated in ethanol (Panreac, Barcelona, Spain), equilibrated with propylene oxide (Merck), and embedded in Epon (Sigma). Semithin and ultrathin sections were prepared with a diamond knife (Diatome, Hatfield, Switzerland) in an LKB ultramicrotome (Leica Microsystems, Weltzlar, Germany). Ultrathin sections were collected on 300 mesh copper grids (Taab, Berks, England), stained with 3 % aqueous uranyl acetate (20 min; BDH, Poole, England) and Reynolds lead citrate (10 min; Merck), and observed in a JEOL 100CXII transmission electron microscope (JEOL, Tokyo, Japan) operated at 60 Kv [69, 70].

Five oocytes with a granular vacuole (two of small and three of medium size) were processed for FISH analysis. Each oocyte was transferred to a 400-μl drop of 1 % sodium citrate (Sigma-Aldrich) in a Petri dish. After 10 min, the swollen cell was allocated to a poly-L-lysine-coated glass slide (Menzel-Glazer, Braunschweig, Germany). Fixation was performed with Carnoy (3:1 *v*/*v* methanol/acetic acid; Merck) by dropping five 10 μl drops starting at 5 cm above with sequential decreases of 1 cm. In this way, the visible vesicle appeared discernible. The slide was then washed for 4 min each in phosphate-buffered saline (PBS; Sigma) and distilled water, dehydrated in ethanol at 70, 96, and 100 % (1 min each), and left to air-dry. It was then incubated at 37 °C in a water bath for 20 min with pepsin (100 μg/ml in water; Sigma) to remove cytoplasmic remnants and enable probe penetration. After a wash in distilled water, it was fixed at 4 °C for 10 min in 1 % de paraformaldehyde (37 % formalin; Sigma) in PBS. The sample was again washed and dehydrated as above and left to air-dry [71–73].

A fluorescent probe mixture was prepared according to manufacturer's instructions (Vysis, Dês Plaines, IL, USA) for chromosomes X, Y, 18, and 21 [7 μl hybridization buffer-LSI + 1 μl CEP18-aqua spectra (blue color) + 1 μl LSI21-orange spectra (red color) + 1 μl CEPX-green spectra + 0.5 μl YSATIII-red spectra + 0.5 μl YSATIII-green spectra (yellow color for the Y chromosome), and 4 μl were applied to each

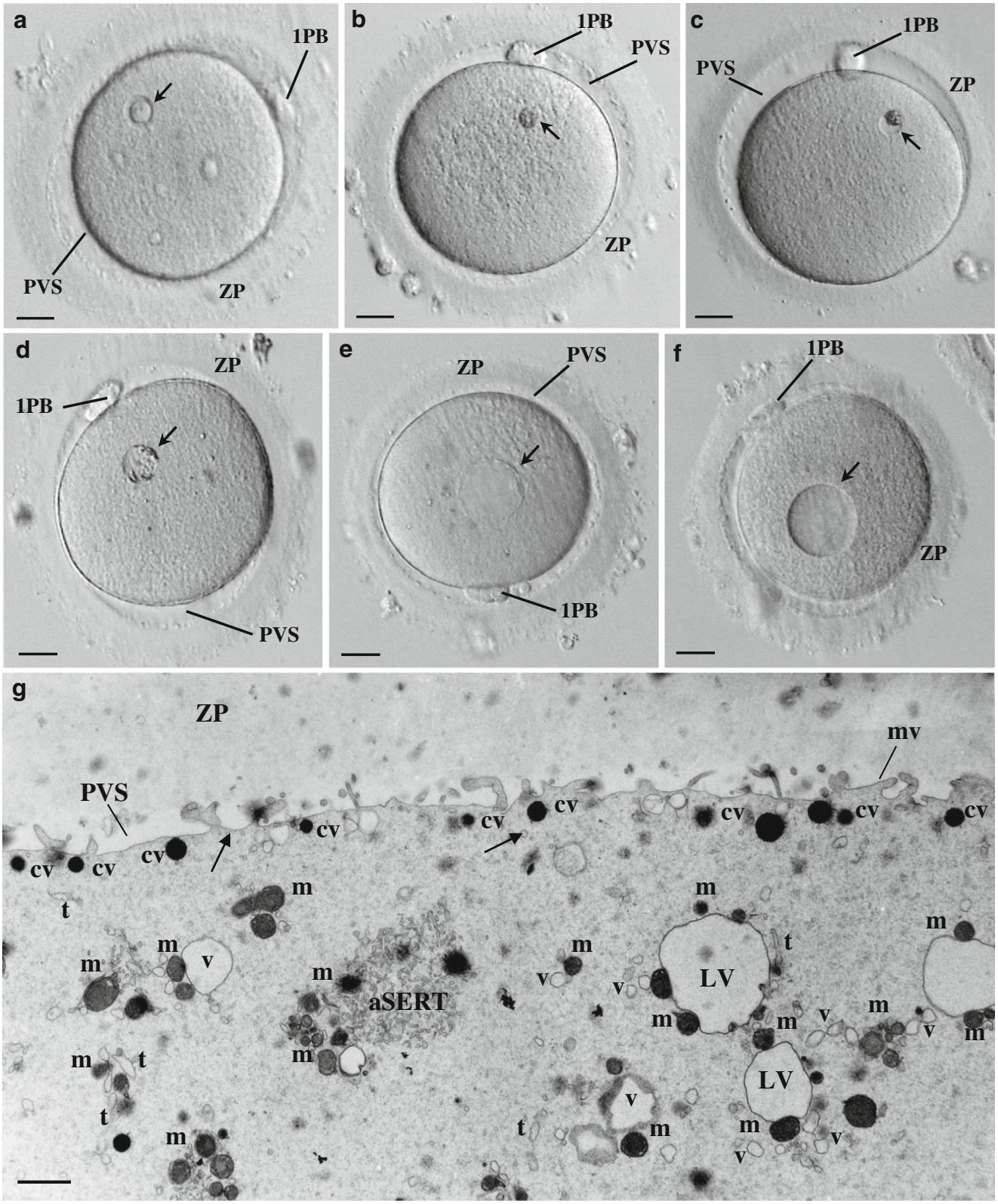

oocyte]. In one case, it was used for the X chromosome 0.5 μl CEPX (DXZ1-spectra aqua) + 0.5 μl CEPX (DXZ1 spectra green) (pink color).

DNA denaturation was performed at 75 °C for 4 min by plating samples in a thermal plate (HYBrite, Vysis, CA, USA), followed by hybridization in a moist dark chamber at

◀ **Fig. 1** Live human mature oocytes observed at the inverted microscope. **a** The bull-eye inclusion (*arrow*) appears as a prominent smooth, moderate dense, round structure surrounded by a cavitated region. Note the zona pellucida (*ZP*), the perivitelline space (*PVS*), and the first polar body (*1PB*). **b** Refractile body (*arrow*). Note the prominent structure made by rough dense materials without evident membrane limits. **c** Small granular vacuole (*arrow*). Note the evident membrane limits and the presence of a large aggregate of rough dense inclusions. **d** Medium-sized granular vacuole (*arrow*). Note the evident membrane limits and the presence of small aggregates of rough dense inclusions around the periphery. **e** Large aggregate of smooth tubular endoplasmic reticulum (*arrow*). This inclusion is generally larger, presents a homogeneous pale content without inclusions, and displays no evident limiting membrane. **f** Vacuole (*arrow*). This inclusion is generally larger, presents a homogeneous pale content without inclusions, and displays an evident limiting membrane. **a**–**f** 20 μm. **g** Ultrastructure of a morphological normal human mature metaphase II oocyte immediately processed after denudation. Note the ZP coat, the narrow PVS, and the short microvilli (*mv*). In the cortex, dense cortical vesicles (*cv*) and tiny smooth endoplasmic reticulum (*SER*) vesicles (*arrows*) can be observed. In the subcortex, small SER vesicles surrounded by one to two mitochondria (*v*), large SER vesicles surrounded by several mitochondria (*LV*), a tubular SER aggregate (*aSERT*), isolated SER tubules (*t*), and isolated mitochondria (*mi*) can be observed. **g** 1 μm

37 °C during 4 h or overnight. Thereafter, samples were washed inside vertical jars for 3 min at 42 °C with 60 % formamide (Fluka, Seelze, Germany) and then with saline sodium citrate (2xSSC) (Invitrogen, Paisley, UK), followed by 4xSSC in 0.05 % Tween-20 (Sigma) at room temperature with shaking. After washing in PBS and distilled water and dehydrated as above, slides were mounted with Vectashield (Vector Laboratories, Burlingame, CA, USA) containing 4′,6-diamidino-2-phenylindole to counterstain DNA and observed in an epifluorescence microscope (AxioImager Z1, Carl Zeiss Inc., New York, USA) [71–73].

Statistical analysis

Statistical analysis was carried out through the IBM SPSS Statistics 20 program for Windows. Means were compared by the *t* test for independent samples. Categorical variables were analyzed using descriptive statistics and chi-square test, with continuity correction. In some variables, in the presence of cells with expected value <5 in contingency tables, the Fisher exact test was used. All statistical tests were two-tailed, with significance level of 0.05 ($p < 0.05$).

Results

Of the 4099 ICSI cycles performed from 2003 till 2013, 11 (0.27 %) exhibited MII oocytes with a bull-eye inclusion and 211 (5.15 %) a granular vacuole. Here, we present the detailed ultrastructural analysis of these dimorphisms, altogether with FISH analysis of granular vacuoles. We then present detailed demographic and stimulation characteristics and full embryological, clinical, and NB outcomes after ICSI treatment of cases with these oocyte dimorphisms.

Inverted microscopy of dimorphic oocytes

At the inverted microscope, the bull-eye inclusion consisted of a prominent smooth round structure surrounded by a short cavitated region (Fig. 1a). Concerning the granular vacuoles, two kinds were observed: the small granular vacuole which showed a discernible membrane and presented a pale appearance and a large aggregate of rough dense inclusions concentrated at one pole or in the middle of the vacuole (Fig. 1c) and the medium-sized granular vacuole which also showed a discernible membrane, had a pale appearance, and presented small dense rough inclusions around the periphery (Fig. 1d). For comparisons to similar dimorphisms, we present images of the refractile body (Fig. 1b), smooth vacuole (Fig. 1e), and vacuole (Fig. 1f).

Electron microscopy of dimorphic oocytes

MII oocytes with a bull-eye inclusion

At the ultrastructural level, oocytes presented a regular ZP, a narrow perivitelline space with short microvilli, and the first polar body. The MII metaphase plate was positioned below the first polar body. Under the oolemma, there was a row of submembranar dense cortical vesicles. The cytoplasm consisted of small moderate dense mitochondria and isolated SER vesicles and tubules. The SER vesicles with associated mitochondria (MV complexes) as well as the aSERT were absent (Fig. 2a–c). The bull-eye inclusion appeared as a prominent structure, without limiting membrane, being surrounded by moderate dense lipid droplets (Fig. 2d, e). Its interior is occupied by small- and medium-sized vesicles with peripheral dense materials. These vesicles presented a double membrane (Fig. 2f). The peripheral crater appearance observed at the live image (Fig. 1a) was not confirmed at semithin sections (Fig. 2a), which showed that the surrounding pale area was due to the presence of light round structures. These light round structures were confirmed at the ultrastructural level to correspond to lipid droplets (Fig. 2d, e).

MII oocytes with small granular vacuoles

At the ultrastructural level (Fig. 3a, b), oocytes presented a regular ZP, a narrow perivitelline space, and short microvilli. The MII metaphase plate was positioned below the first polar body (not shown). Under the oolemma, there was a row of submembranar dense cortical vesicles. The ooplasm consisted of small moderate dense

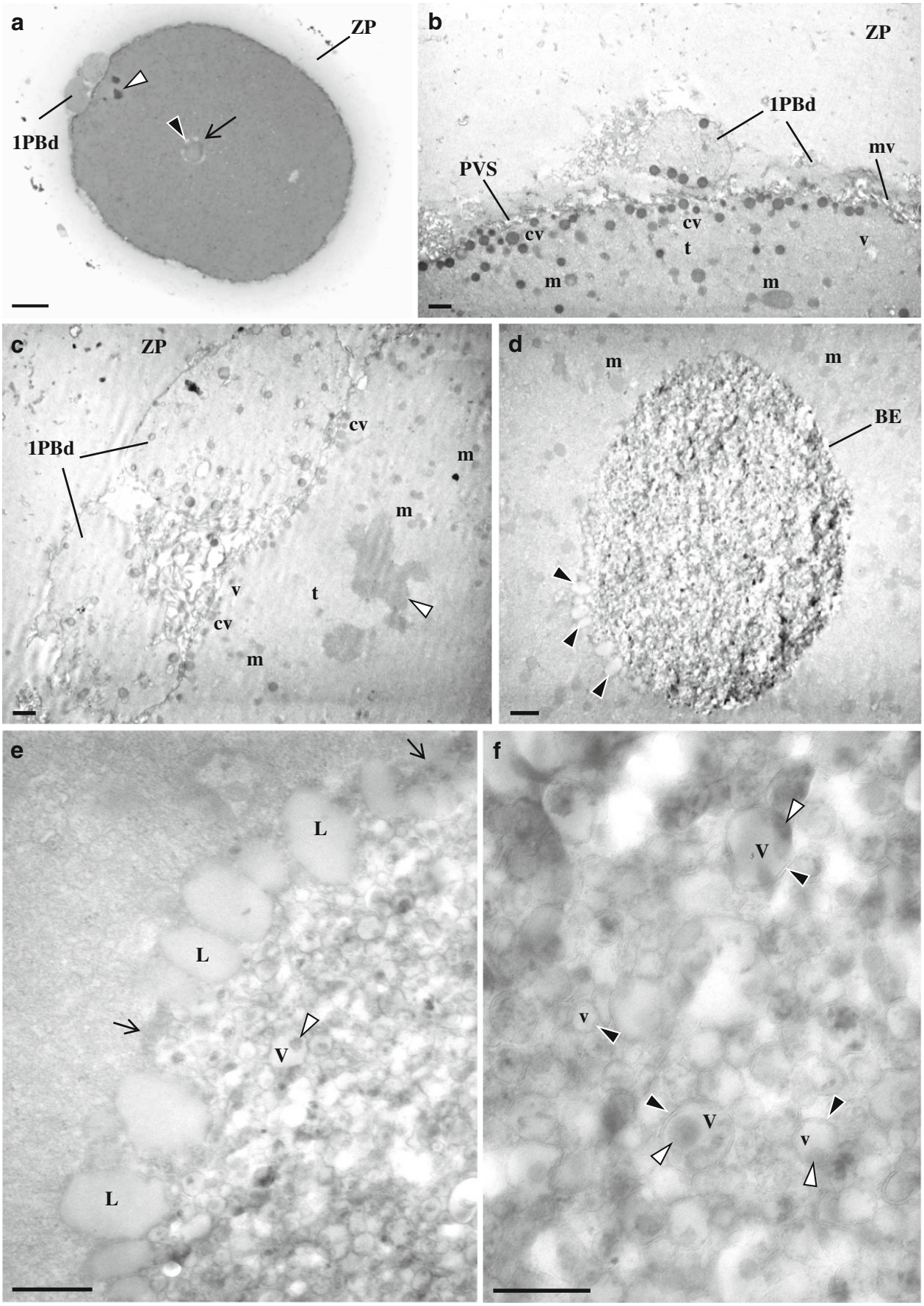
a
ZP
1PBd
b
ZP
1PBd
mv
PVS
cv
cv
t
v
m
m
c
ZP
cv
1PBd
m
m
v
t
cv
m
d
m
m
BE
e
L
L
V
L
f
V
v
V
v

◀ **Fig. 2** Ultrastructure of human mature oocyte with bull-eye inclusion. **a** Semithin section. Note the zona pellucida (*ZP*), the metaphase II plate (*white arrowhead*), and the first polar body that is divided (*1PBd*). The bull-eye inclusion (*arrow*) is surrounded by several light round structures (*black arrowhead*). **b**–**f** Ultrathin sections. **b**, **c** The oocyte cortex contains cortical vesicles (*cv*), isolated smooth endoplasmic reticulum (*SER*) vesicles (*v*) and tubules (*t*), and moderate dense mitochondria (*m*). Note the ZP, the perivitelline space (*PVS*), microvilli (*mv*), the 1PBd, and the metaphase II plate (*white arrowhead*). **d** The bull-eye inclusion (*BE*) presents prominent contents and is surrounded by lipid droplets (*black arrowheads*). **e** The surface of the inclusion is devoid of a limiting membrane (*arrows*) and is surrounded by moderate dense lipid droplets (*L*). The interior of the inclusion is made of medium and small vesicles (*V*). Medium vesicles present an internal dense amorphous structure at one of the poles (*white arrowhead*). **f** The vesicles of the inclusion appear delimited by a double membrane (*black arrowheads*). **a** 20 μm. **b**–**d** 1 μm. **e** 0.5 μm. **f** 0.25 μm

mitochondria, isolated SER vesicles and tubules, and aSERT. Small and large MV complexes were absent (Fig. 3b). The periphery of the small granular vacuole presented regions in contact with the cytoplasm, regions delimited by a single membrane, and regions delimited by a double membrane (Fig. 3c, d). Structures resembling nuclear pores could also be observed (Fig. 2g inset). The interior had a fine fibrillar appearance and contained a large lipid droplet. At the free borders, the granular vesicle showed signs of incorporation of moderate dense lipid droplets, vesicles with floccular contents and dense vesicles with double membrane and tubular cristae (Fig. 3c inset).

MII oocytes with medium-sized granular vacuoles

At the ultrastructural level (Fig. 4a–c), these oocytes presented a regular ZP, a narrow perivitelline space, and short microvilli. The MII metaphase plate was positioned below the first polar body (not shown). Under the oolemma, there was a row of submembranar dense cortical vesicles. The ooplasm contained small moderate dense mitochondria, isolated small SER vesicles, small MV complexes, and aSERT. The cytoplasm appeared enriched in isolated SER tubules. Large MV complexes were absent (Fig. 4a–c). The periphery of the granular vacuole presented regions in contact with the cytoplasm, regions delimited by a single membrane, and regions delimited by a double membrane (Fig. 4d–f). The interior had a fine fibrillar appearance, and at its center, there was a moderate dense granulo-fibrillar structure. At the free borders, it was observed there was the inclusion of moderate dense lipid droplets surrounded by very dense materials and the incorporation of very dense round structures (Fig. 4d, e). At other points of the granular vacuole periphery, the granular vacuole membrane appeared to originate protrusions (Fig. 4f).

Fluorescent in situ hybridization of oocytes with granular vacuoles

The ultrastructural morphology of granular vacuoles raised the suspicion that they could represent degenerative micronuclei. Thus, for this dimorphism, we performed FISH analysis. This analysis revealed the presence of chromosome signals in granular vacuoles. Fluorescent signals in the polar body indicated that they were diploid, meaning that they had already replicated. Fluorescent signals in metaphase plates revealed haploid and diploid (replicated) constitutions, with one showing monosomy. Fluorescent signals in granular vacuoles indicated a diploid constitution, with cases of monosomy and trisomy (Figs. 5 and 6).

Clinical outcomes

From the 4099 consecutive ICSI treatment cycles, three study groups were established. Controls were those ICSI cycles without bull-eye or granular vacuole dimorphisms (3877 cycles), the bull-eye group corresponded to ICSI cycles with presence of at least one oocyte with this dimorphism (11 cycles), and the granular vacuole group corresponded to ICSI cycles with presence of at least one oocyte with this dimorphism (211 cycles). The rate of appearance of these dimorphisms during 10 consecutive years was 0.27 % for the bull-eye inclusion and 5.15 % for the granular vacuole.

Regarding the *bull-eye inclusion* (Table 1), there were no significant differences in demographic (patient age, time of infertility, factors of infertility, and basal FSH) and stimulation (mean number of follicles, mean total gonadotropin dose, mean time of stimulation, mean serum estradiol levels, and mean hCG dose) characteristics as well as in relation to embryological, clinical, or NB (gestation age and NB weight) outcomes. No cases of NB malformations were noticed. Of the 11 cycles with bull-eye inclusion, there were 10 embryo transfer cycles (ETC). Of these, eight were with embryos derived from normal oocytes (normal ETC) from which four healthy NB were obtained, one was with embryos derived one from a normal oocyte and another from a dimorphic oocyte (mixed ETC) from which resulted one healthy NB, and one was with embryos derived from dimorphic oocytes (pure ETC) from which no CP was observed.

In relation to *granular vacuoles* (Table 1), there were no significant differences regarding patient characteristics except for a significantly lower mean male age. In relation to stimulation characteristics, there was significantly higher mean number of follicles and of estradiol levels, associated with significantly lower total gonadotropin dose used. Regarding embryological outcomes, there was significantly higher mean number of retrieved oocytes, oocyte maturation rate, and FR, associated with a significantly lower ECR. There were no significant differences in relation to clinical and NB outcomes,

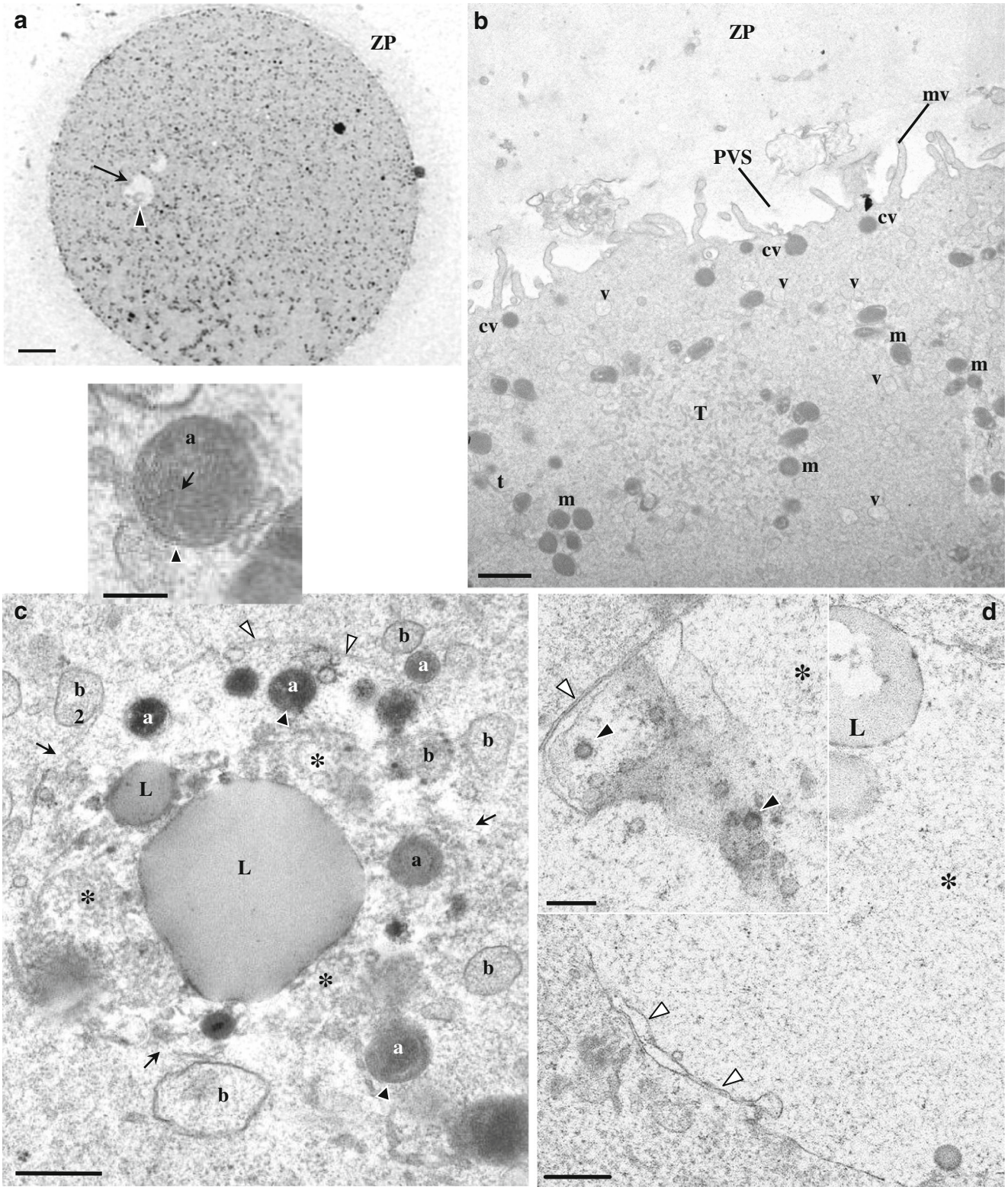

with exception of a significantly higher abortion rate. There were no cases of NB malformations.

Of the 211 cycles with granular vacuoles, there were 203 ETC. Of these, there were 141 cycles with normal ETC, 52 cycles with mixed ETC, and 10 cycles with pure ETC. In relation to demographic parameters, normal ETC cycles showed significantly lower mean male age and basal FSH levels, mixed ETC cycles evidenced significantly higher mean

◀ **Fig. 3** Ultrastructure of human mature oocyte with a small granular vacuole. **a** Semithin section. The inclusion appears as a round structure with a pale appearance (*arrow*), and at one pole, there is the presence of an aggregate of moderate dense material (*black arrowhead*). Note the zona pellucida (*ZP*). **b**–**d** Ultrathin sections. **b** At the oocyte cortex, cortical vesicles (*cv*), isolated smooth endoplasmic reticulum (*SER*) vesicles (*v*) and tubules (*t*), a SER tubular aggregate (*T*), and moderate dense mitochondria (*m*) can be observed. Note the perivitelline space (*PVS*) and microvilli (*mv*). **c** The granular vacuole presents regions delimited by a membrane (*white arrowheads*) and regions with membrane disruption (*arrows*). The interior of the granular vacuole presents a fine fibrillar appearance (*asterisk*). Within the granular vacuole, there are small dense vesicles (*a*) with a double membrane and cristae (*black arrowheads*; also see inset), small vesicles with fine fibrillar materials (*b*), small lipid droplets (*L*), and a very large lipid droplet (*L*). **d** Periphery of the granular vacuole (*asterisk*). Note regions with double membrane (*white arrowheads*). Similar structures to nuclear pores (*black arrowheads*) could also be observed (*inset*). **a** 20 μm. **b** 1 μm. **c** 0.5 μm. Inset in **c** 0.25 μm. **d** 0.5 μm. Inset in **d** 0.25 μm

female age, and pure ETC cycles showed significantly higher basal FSH levels. Regarding stimulation characteristics, normal ETC cycles showed a significantly higher number of follicles and of estradiol levels and significantly lower total gonadotropin and hCG doses used. On the contrary, cycles with mixed ETC evidenced a significantly higher total gonadotropin and hCG doses used. No significant differences were observed for cycles with pure ETC. In relation to embryological outcomes (Table 2), normal ETC showed a significantly higher mean number of collected oocytes and FR, associated with a significantly lower ECR, mixed ETC evidenced lower ECR, and pure ETC presented a significant increase in oocyte maturation rate. Regarding clinical outcomes (Table 2), normal ETC cycles showed significantly higher rates of biochemical pregnancy and CP, as well as significantly higher IR and LBDR, mixed ETC presented a significantly lower IR and NB rates, and no significant differences were observed for cycles with pure ETC. A significant increase in the abortion rate was observed in all three subgroups of ETC. No significant differences were found regarding NB characteristics and no case of NB malformations was detected. Of note, these clinical outcomes were obtained when analyzing data within each type of ETC: normal ETC (141), mixed ETC (52), and pure ETC (10). However, when rates were calculated to the total number of ETC (203), the values for mixed and pure ETC were completely different. Significantly lower biochemical pregnancy, CP, OP, LBDR, and NB rates were obtained (Table 2).

Discussion

We here describe two not previously characterized oocyte cytoplasmic dimorphisms, the bull-eye inclusion and the granular vacuole.

Regarding patient karyotypes, our results (Suppl. Karyotype information) confirm that infertile patients present a higher rate of abnormal karyotypes than the general or fertile populations [74–83]. Patients whose oocytes displayed the bull-eye dimorphism presented no abnormal karyotypes. On the contrary, the presence of granular vacuoles in oocytes was associated with a higher rate of female karyotype abnormalities, suggesting a relationship between female karyotype abnormalities and the presence of this dimorphism.

The bull-eye dimorphism was present in 0.27 % of 4099 consecutive ICSI treatment cycles. It is devoid of a delimiting membrane being thus an inclusion. It is surrounded by lipid droplets and contains an aggregate of small vesicles with double membrane and eccentric dense amorphous materials. The aggregation of the small vesicles is so marked that creates a prominent structure visible in the live images. We are unable, at the moment, to explain the reason for this aggregation or the presence of a double membrane in the small vesicles. This aggregation can be a way to remove an abnormal excess of endocytic vesicles or Golgi vesicles assembled during oocyte maturation. These vesicles can also correspond to the retention of those SER components that are absent from the oocyte. In fact, the MV complexes and aSERT usually required for calcium oscillations and oocyte activation [27, 84] were absent from these dimorphic oocytes. The absence of significance to female age, female factors of infertility, and basal FSH suggests that this dimorphism may not be associated with aged ovaries. Absence of significance regarding stimulation characteristics also suggests that this dimorphism is not a consequence of ovarian stimulation. Moreover, the absence of significance to embryological outcomes proposes that this dimorphism does not impair fertilization and embryo development, as well as clinical outcomes or NB characteristics. However, as the absence of critical SER elements would not allow normal embryo development, the observed normal outcomes were probably due to the transfer of embryos without this dimorphism (normal ETC and mixed ETC). In fact, of the eight NB, four derived from normal ETC and 1 from mixed ETC but the unique case with pure ETC resulted in pregnancy absence. Intriguingly, in this pure ETC, no female factors were evident. Three MII oocytes fertilized and originated a 4AB embryo that was transferred at day 2. This means that the oocyte was activated even in the absence of the known SER critical elements.

The *granular vacuoles* appeared in 5.15 % of 4099 consecutive ICSI treatment cycles, in 2.71 % of the 111 cycles with at least one oocyte displaying a medium-sized granular vacuole, and in 2.44 % of the 100 cycles with at least one oocyte presenting a small granular vacuole. At the ultrastructural level, these granular vacuoles presented regions delimited by a double membrane and contained fine granulo-fibrillar materials. Granular vacuoles also incorporated lipid droplets, dense materials, dense round structures, and

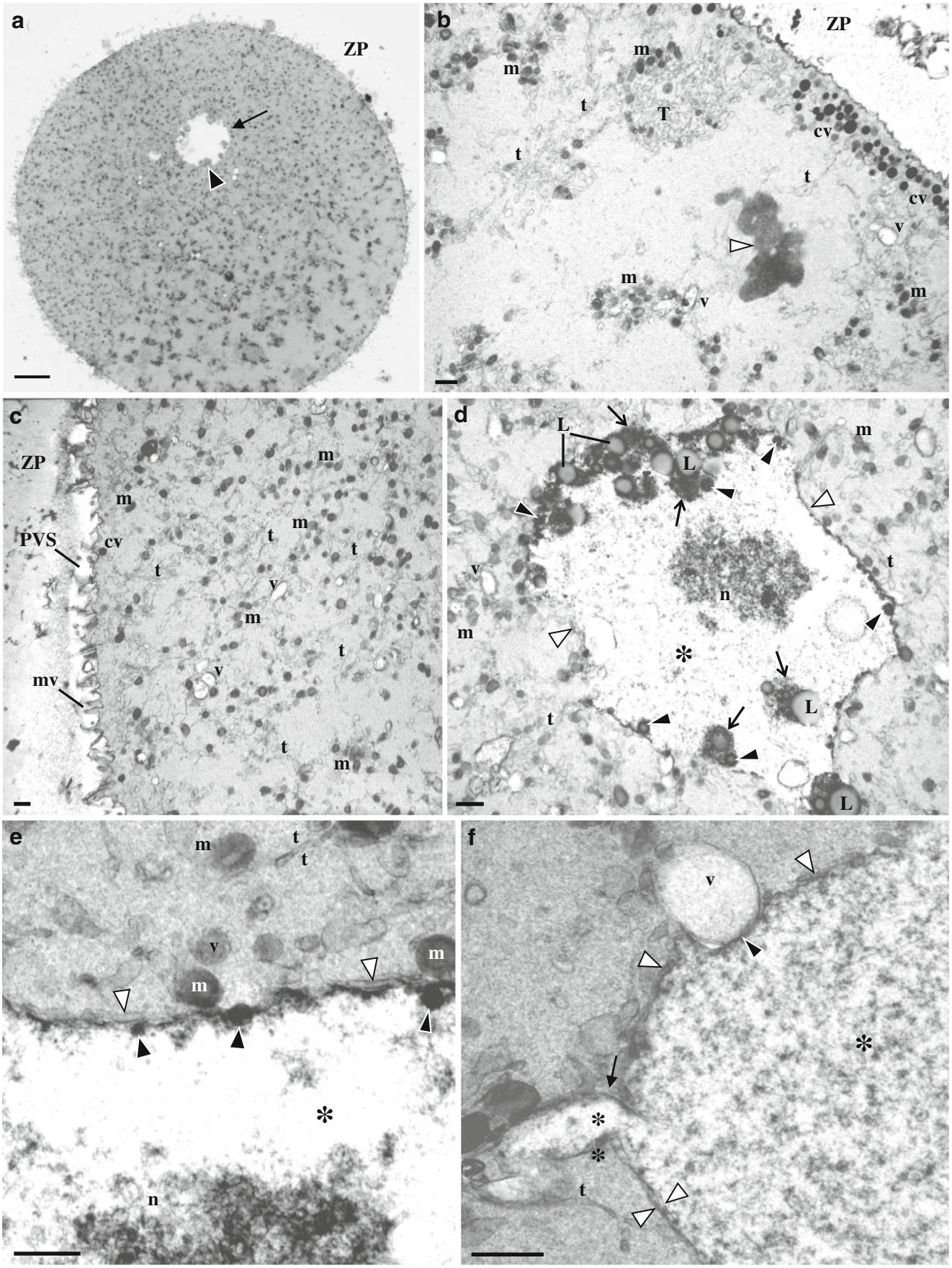
a
ZP
b
ZP
m
m
t
T
t
cv
t
cv
v
m
v
m
c
ZP
m
m
PVS
cv
m
t
t
t
v
m
t
mv
v
t
m
d
L
L
m
v
n
m
t
L
L
e
m
t
t
v
m
m
n
f
v
t

◀ **Fig. 4** Ultrastructure of human mature oocyte with a medium-sized granular vacuole. **a** Semithin section. This vesicle appears as a round pale structure (*arrow*) with peripheral inner small aggregates of materials with moderate density (*black arrowhead*). Note de zona pellucida (*ZP*). **b**–**f** Ultrathin sections. **b** At the oocyte cortex, there are cortical vesicles (*cv*), smooth endoplasmic reticulum (*SER*) isolated vesicles (*v*) and tubules (*t*), a SER tubular aggregate (*T*), and moderate dense mitochondria (*m*). Note the metaphase II plate (*white arrowhead*). **c** Oocyte cortex and subcortex. Note the abundance of SER isolated tubules and mitochondria, small MV complexes, the perivitelline space (*PVS*), and microvilli (*mv*). **d** The granular vacuole presents regions delimited by a membrane (*white arrowheads*). At the periphery, there is inclusion of moderate dense lipid droplets (*L*) associated to dense materials (*arrows*). There is also inclusion of small round dense structures (*black arrowheads*). The interior of the granular vacuole presents a fine fibrillar appearance (*asterisk*) with a granulo-fibrillar dense region at the center (*n*). **e** Periphery of the granular vacuole. Note regions with double membrane (*white arrowheads*), the dense cover of the inner membrane, and the associated small round dense structures (*black arrowheads*). **f** Periphery of the granular vacuole. Note regions with double membrane (*white arrowheads*), a granular vacuole protrusion (*arrow*), and a granular vacuole indentation (*black arrowhead*) in association with a vesicle (*v*) containing floccular contents. **a** 20 μm. **b**–**d** 1 μm. **e** 0.5 μm. **f** 05 μm

dense mitochondria. As these observations suggested that granular vacuoles could correspond to degenerative micronuclei, we performed FISH analysis and found chromosome signals, thus indicating that granular vacuoles probably correspond to pyknotic nuclei.

The present theories regarding the development of micronuclei refer mitotic or meiotic errors that induce an abnormal distribution of chromosomes, chromosome mal-separation, fragmentation, or abnormal replication, followed by incorporation of chromosomes in micronuclei for later reabsorption. In either case, micronuclei reflect damage of genomic material [85–87]. In our results, although most of the metaphase plates showed a normal chromosomal complement and granular vacuoles a diploid constitution, an abnormal chromosomal constitution cannot be ruled out as we have only examined a restricted number of chromosomes. As pure ETC displayed abnormal rates of embryo development, it is thus possible that granular vesicles correspond to the abnormal incorporation of chromosomes occurring during oogenesis as previously described [85–87]. These granular vacuoles may then suffer degeneration associated with incorporation of other cytoplasmic elements, resembling as consequence an autophagy vacuole.

The cytoplasmic characteristics of dimorphic oocytes were not due to aging, since oocytes were processed immediately after denudation. Additionally, the presence of micronuclei was not a consequence of oocyte activation, as these dimorphic oocytes presented a single polar body, the metaphase plate, and cortical vesicles, which are the characteristics of a fresh mature human oocyte. Furthermore, besides the detection of DNA in granular vacuoles, the polar body and the metaphase plate were recovered and confirmed to contain chromosome signals.

When compared to normal MII oocytes [70], oocytes with granular vacuoles showed absence of large MV complexes, the SER components usually required for calcium oscillations and oocyte activation [27, 84]. Even though other authors have considered that large MV complexes can only be observed in aged oocytes [49, 51], we have no plausible explanation for this association. Granular vacuoles did not affect nuclear maturation and the cytoplasm also showed no other signs of immaturity. This is contrary to previous observations that indicated that nuclear maturity parallels cytoplasmic maturation [8, 88]. Although abnormal SER organization has been related to higher female age, ovarian stimulation, and oocyte aging during prolonged culture [49, 51], in the present case, there were no relationships with female age, stimulation, oocyte maturation, or oocyte aging (oocytes were processed immediately after denuding and inspection at the inverted microscope). The absence of significant differences regarding female age, time of infertility, female infertility factors, and basal FSH suggests that the appearance of granular vacuoles seems to be independent of female characteristics. In relation to stimulation parameters, cycles with this dimorphism presented higher number of follicles and estradiol levels associated with significantly lower total gonadotropin dose used. This could explain the observed significantly higher mean number of retrieved oocytes and maturation rate, suggesting that the presence of granular vacuoles may be related to ovarian stimulation. The fertilization rate was also not affected, probably meaning that calcium originated from other stores was sufficient to ensure oocyte activation. On the other hand, the low ECR and the high abortion rate could be related to an abnormal constitution of the metaphase plate due to oogenesis mitotic or meiotic errors with incorporation of displaced chromosomes in micronuclei that then entered degeneration [85–87].

We found no previous reports on the clinical outcomes of cycles containing oocytes with the bull-eye dimorphism. Because of the rarity of this dimorphism, we had few clinical cycles to evaluate. Nevertheless, as these oocytes showed abnormal SER components, with absence of aSERT and MV complexes, it can be inferred that pure ETC will not enable a successful pregnancy.

We found several reports on dimorphisms that exhibited some morphological similarities to granular vacuoles and that were described as intracellular degeneration (intracellular necrosis or cytolysis). In one of these studies, the dimorphic feature described represented 3 % of the cytoplasmic dimorphisms and appeared delimited by an incomplete double membrane, and the interior presented a granular appearance with lipid droplets and vesicles [1]. In another work, authors observed small membrane-limited vesicles containing dense inclusions. These

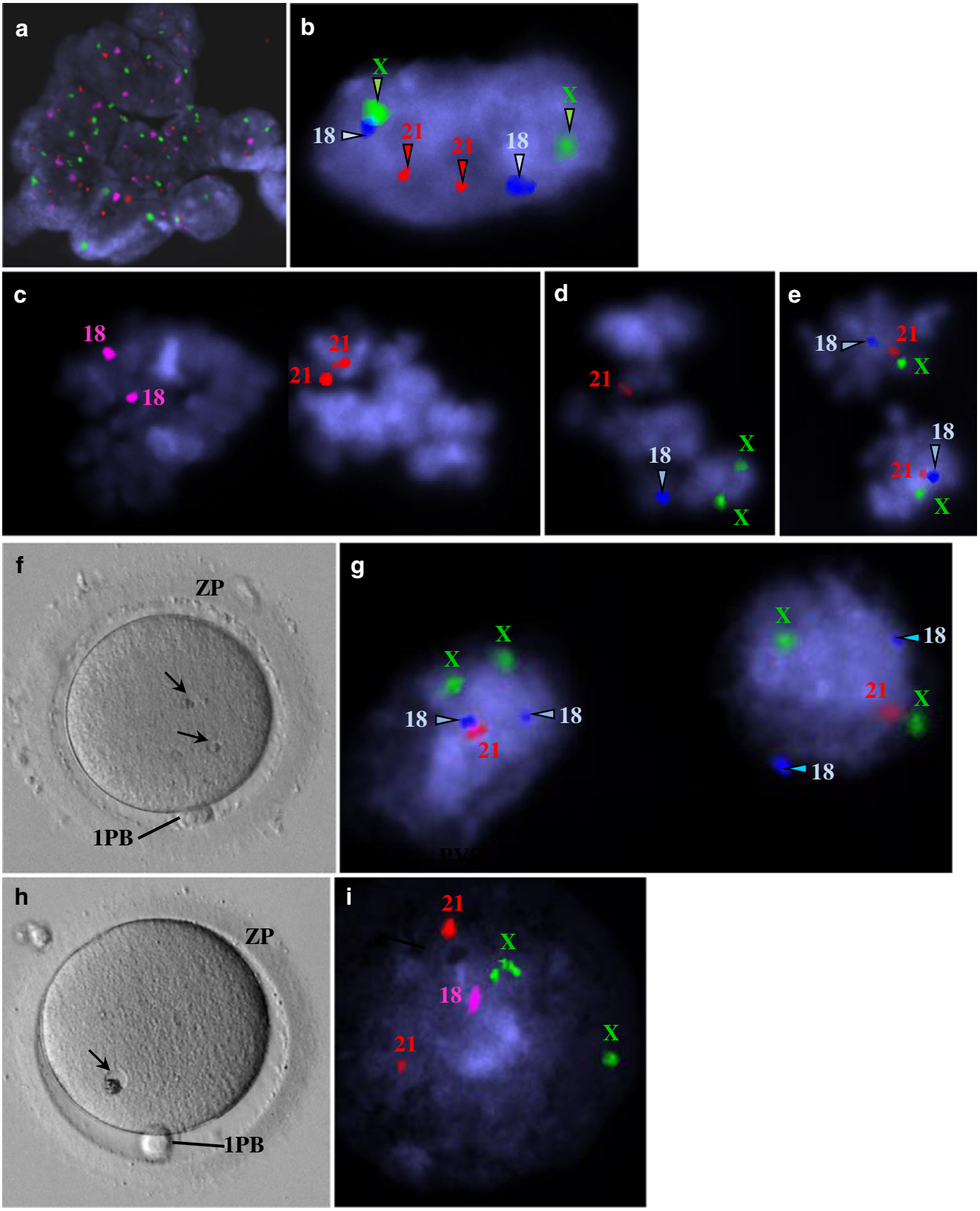
a
b
X
18
21
21
18
X
c
18
18
21
21
d
21
18
X
X
e
18
21
X
18
21
X
f
ZP
1PB
g
X
X
18
18
21
X
18
21
X
18
h
ZP
1PB
i
21
X
18
21
X

◀ **Fig. 5** Images from epifluorescence microscopy using fluorescent in situ hybridization (FISH) analysis of human mature oocytes for detection of chromosomes X, 18, and 21 (**a**–**e**, **g**, **i**). Live human mature oocytes with small granular vacuoles observed at the inverted microscope (**f**, **h**). **a** Residual follicular cells were present in one case and showed a diploid constitution (XX,1818,2121). X (*green*), 18 (*pink*), 21 (*red*). **b** Polar body from one case showing a diploid constitution (XX,1818,2121). X (*green*), 18 (*blue*), 21 (*red*). **c**–**e** Metaphase II from three cases. **c** Diploid constitution due to probable replication associated with monosomy X (X,1818,2121). X (*green*), 18 (*pink*), 21 (*red*). **d** Haploid constitution with replication of chromosome X (XX,18,21). X (*green*), 18 (*blue*), 21 (*red*). **e** Diploid constitution due to probable replication (XX,1818,2121). X (*green*), 18 (*blue*), 21 (*red*). **f** Mature oocyte showing two small granular vacuoles. **g** Both small granular vacuoles showed a diploid constitution with monosomy 21 (XX,1818,21). X (*green*), 18 (*blue*), 21 (*red*). **h** Mature oocyte showing a small granular vacuole. **i** The small granular vacuole shows a diploid constitution with monosomy 18 (XX,18,2121). X (*green*), 18 (*pink*), 21 (*red*)

oocytes were able to fertilize and gave origin to normal embryos but then underwent embryo development arrest at the morula stage [2]. Finally, an additional study described an inclusion containing several scattered dark bodies (presumably chromatin) that were argued to represent pyknotic nuclei [33]. In all these cases, and contrary to our results, the dimorphic oocytes showed a normal distribution of SER organelles.

Conclusion

Embryos transferred that are not exclusively derived from bull-eye dimorphic oocytes seem not to be associated with poor clinical outcomes. However, if the transferred embryos are exclusively derived from oocytes containing the bull-eye inclusion, it is expected that they will not

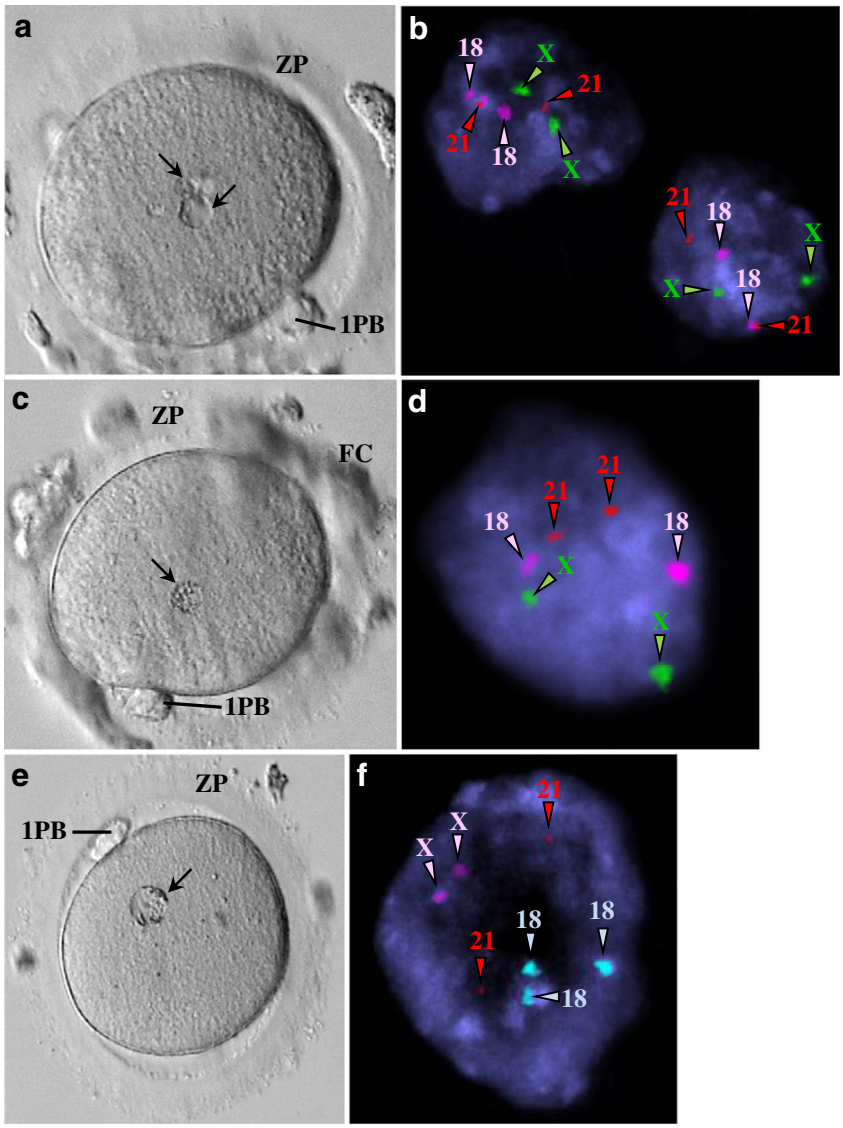

Fig. 6 Images from epifluorescence microscopy using fluorescent in situ hybridization (FISH) analysis of human mature oocytes for detection of chromosomes X, 18, and 21 (**b**, **d**, **f**). Live human mature oocytes with medium-sized granular vacuoles observed at the inverted microscope (**a**, **c**, **e**). **a** Mature oocyte showing two medium-sized granular vacuoles. **b** Both medium-sized granular vacuoles show a diploid constitution (XX,1818,2121). X (*green*), 18 (*pink*), 21 (*red*). **c** Mature oocyte showing a medium-sized granular vacuole. **d** The medium-sized granular vacuole shows a diploid constitution (XX,1818,2121). X (*green*), 18 (*pink*), 21 (*red*). **e** Mature oocyte showing a medium-sized granular vacuole. **f** The medium-sized granular vacuole shows a diploid constitution (XX,1818,2121). X (*green*), 18 (*blue*), 21 (*red*)

Table 1 Embryological and clinical outcomes from oocytes with granular vacuole or bull-eye inclusion

Parameters	Controls	Granular vacuole	Bull-eye inclusion	*p*
Cycles (*n*)	3877	211	11	
COC (mean, range)	7.0 ± 4.8 0–42	9.2 ± 4.8 1–26	6.9 ± 2.9 3–12	a
Maturation rate	78.3	80.5	86.8	a
Fertilization rate	77.2	82.8	80.3	a
Embryo cleavage rate	99.2	93.4	100	a
Day 3 grade A/B rate	95.5	96.2	100	NS
Blastocyst rate	47.6	50.4	46.2	NS
Embryo transfer cycles (*n*)	3352	203	10	
No. of embryos transferred (mean, rate)	1.9 ± 0.5 1–4	1.8 ± 0.5 1–3	2.0 ± 0.5 1–3	NS
Biochemical pregnancy (rate per ETC)	40.7	46.3	40	NS
Clinical pregnancy (rate per ETC)	36.7	42.9	30	NS
Implantation rate	24.8	27.8	25	NS
Abortion (rate per CP)	11.7	20.7	0	a
OP (rate per ETC)	31.7	34.0	30	NS
LBDR (rate per ETC)	29.2	32.5	30	NS
Newborn (rate per ETC)	1218 (36.3)	75 (36.9)	5 (50)	NS

Values in *n*, rate, mean ± SD, or range. Significance ($p < 0.05$)

Controls ICSI cycles in which mature metaphase II oocytes did not display a granular vacuole or a bull-eye inclusion, *Granular vacuole* ICSI cycles in which at least one of the oocytes had a granular vacuole, *Bull-eye inclusion* ICSI cycles in which at least one of the oocytes displayed a bull-eye inclusion, *a* controls vs granular vacuole, *b* controls vs bull-eye inclusion, *c* granular vacuole vs bull-eye inclusion, *NS* not significant, *COC* cumulus-oocyte complexes (aspirated oocytes), *ETC* embryo transfer cycles, *CP* clinical pregnancy, *OP* ongoing pregnancy, *LBDR* live birth delivery rate, *NB* newborn

enable a successful pregnancy. If the embryos transferred are from oocytes without granular vacuoles, although coming from a cohort containing dimorphic oocytes, the clinical outcomes seem not to be prejudiced. However, the transfer of embryos derived from oocytes with granular vacuoles, either mixed or pure, is associated with

Table 2 Embryological and clinical outcomes from oocytes with Granular vacuole

Parameters	Controls	Oocytes with granular vacuole (total)			*p*
		Cycles with ET of normal MII	Cycles with mixed ET	Cycles with pure ET	
Embryo transfer cycles (*n*)	3352	141	52	10	203
COC (mean, rate)	7.6 ± 4.6 1–42	10.2 ± 4.7 2–26	7.2 ± 3.6 2–23	4.9 ± 3.7 1–13	a
Maturation rate	79.1	81.0	79.0	91.8	c
Fertilization rate	77.8	83.6	81.6	73.3	a
Embryo cleavage rate	99.2	93.0	94.6	97.0	a, b
Day 3 grade A/B rate	95.6	95.8	97.1	100	NS
Blastocyst rate	49.0	51.3	51.9	29.4	NS
No. of embryos transferred (mean, rate)	1.9 ± 0.5 1–4	1.8 ± 0.5 1–3	2.1 ± 0.4 1–3	1.3 ± 0.5 1–2	a, b, c
Biochemical pregnancy (rate per ETC)	40.7	51.1 (35.5)	34.6 (8.9)	40.0 (2.0)	a
Clinical pregnancy (rate per ETC)	36.7	47.5 (33.0)	30.8 (7.9)	40.0 (2.0)	a, B, C
Implantation rate	24.8	32.4	16.2	38.5	a, b
Abortion (rate per CP)	11.7	20.9	31.3	50.0	a, b, c
OP (rate per ETC)	31.7	37.6 (26.1)	21.2 (5.4)	20.0 (1.0)	NS, B, C
LBDR (rate per ETC)	29.2	37.6 (26.1)	21.2 (5.4)	20.0 (1.0)	a, B, C
Newborn (rate per ETC)	1218 (36.3)	61 (43.3) (30.0)	12 (23.1) (5.9)	2 (20.0) (1.0)	b, B, C

Values in *n*, rate, mean ± SD, or range. Significance ($p < 0.05$)

Controls ICSI cycles in which mature metaphase II oocytes (MII) did not display a granular vacuole (GRVa), *Oocytes with granular vacuole* ICSI cycles in which at least one of the oocytes had a GRVa, *Cycles with ET of normal MII* ICSI cycles in which at least one of the oocytes had a GRVa and where embryos transferred derived from MII oocytes without GRVa, *Cycles with mixed ET* ICSI cycles in which at least one of the oocytes had a GRVa and where embryos transferred consisted in one derived from a MII oocyte without GRVa and one MII oocyte with GRVa, *Cycles with pure ET* ICSI cycles in which at least one of the oocytes had a GRVa and where embryos transferred derived from MII oocytes with GRVa, *a* control cycles vs cycles with ET of normal MII (141 ETC), *b* control cycles vs cycles with mixed ET (52 ETC), *c* control cycles vs cycles with pure ET (10 ETC), *A* control cycles vs cycles with ET of normal MII (203 ETC), *B* control cycles vs cycles with mixed ET (203 ETC), *C* control cycles vs cycles with pure ET (203 ETC), *NS* not significant, *COC* cumulus-oocyte complexes (aspirated oocytes), *ETC* embryo transfer cycles, *CP* clinical pregnancy, *OP* ongoing pregnancy, *LBDR* live birth delivery rate, *NB* newborn

high abortion rates and very poor clinical outcomes. The bull-eye inclusion and granular vacuoles might thus be used as new prognostic factors for clinical outcomes.

Acknowledgments The authors would like to that the following persons: for oocyte retrieval to Jorge Beires, MD, PhD, Specialist in Gynecology and Obstetrics, from the Department of Gynecology and Obstetrics, Director of the Unit of Gynecology and Reproductive Medicine, Hospital of S. John, E.P.E., Porto, Portugal and José Manuel Teixeira da Silva, MD, Specialist in Gynecology and Obstetrics; for anesthesiology to José Correia, MD, Anesthetist (Department of Anesthesiology, Hospital of S. John, E.P.E., Porto, Portugal); for IVF laboratorial work assistance to Paulo Viana, MSc., Biologist, Clinical Embryologist and Nuno Barros MSc., Microbiologist (CGR-ABarros); for spermiology laboratorial work to Ana Gonçalves, MSc., Biochemist and Cláudia Osório MSc., Biologist (CGR-ABarros); for technical support on FISH analysis to Ana Raquel Azevedo, Ph.D. (ICBAS-UP); and for transmission electron microscopy technical support to Célia Soares, M.D. and Ângela Alves, BSc., Technical assistant for teaching and research (ICBAS-UP).

We also would like to thank all colleagues from the many other research articles, reviews, book chapters, and books that we did not cite in this manuscript but whose lecture was fundamental to the writing of the present manuscript.

Funding UMIB is funded by National Funds through FCT-Foundation for Science and Technology, under the Pest-OE/SAU/UI0215/2014.

Compliance with ethical standards The authors declare that they have followed all the rules of ethical conduct regarding originality, data processing and analysis, duplicate publication, and patient treatments.

Conflict of interest The authors declare that they have no competing interests.

Informed consent Informed consent was obtained from all individual participants included in the study.

References

1. Van Blerkom J. Occurrence and developmental consequences of aberrant cellular organization in meiotically mature human oocytes after exogenous ovarian hyperstimulation. J Elect Microsc Techn. 1990;16:324–46.
2. Van Blerkom J, Henry G. Oocyte dysmorphism and aneuploidy in meiotically mature human oocytes after ovarian stimulation. Hum Reprod. 1992;7:379–90.
3. Magli NC, Jones GM, Lundi K, Van den Abbeel E, The ESHRE Special Interest Group on Embryology. Atlas of human embryology: from oocytes to preimplantation embryos. Hum Reprod. 2012;27 Suppl 1:1–91.
4. Sundström P, Nilsson BO. Meiotic and cytoplasmic maturation of oocytes collected in stimulated cycles is asynchronous. Hum Reprod. 1988;3:613–9.
5. Ebner T, Moser M, Sommergruber M, Tews G. Selection based on morphological assessment of oocytes and embryos at different stages of preimplantation development. Hum Reprod Update. 2003;9:251–62.
6. Ebner T, Moser M, Tews G. Is oocyte morphology prognostic of embryo developmental potential after ICSI? Reprod BioMed Online. 2006;12:507–12.
7. Rienzi L, Vajta G, Ubaldi F. Predictive value of oocyte morphology in human IVF: a systematic review of the literature. Hum Reprod Update. 2011;17:34–45.
8. Keef D, Kumar M, Kalmbach K. Oocyte competency is the key to embryo potential. Fertil Steril. 2015;103:317–22.
9. Ebner T, Balaban B, Moser M, Shebl O, Urman B, Ata B, et al. Automatic user-independent zona pellucida imaging at the oocyte stage allows for the prediction of preimplantation development. Fertil Steril. 2010;94:913–20.
10. Shi W, Xu B, Wu L-M, Jin R-T, Luan H-B, Luo L-H, et al. Oocytes with a dark zona pellucida demonstrate lower fertilization, implantation and clinical pregnancy rates in IVF/ICSI cycles. PLoS One. 2014;9:e89409. doi:10.1371/journal.pone.0089409.
11. Sauerbrun-Cutler M-T, Vega M, Breborowicz A, Gonzales E, Stein D, Lederman M, et al. Oocyte zona pellucida dysmorphology is associated with diminished in-vitro fertilization success. J Ovarian Res. 2015;8:5. doi:10.1186/s13048-014-0111-5.
12. Sousa M, Teixeira da Silva J, Silva J, Cunha M, Viana P, Oliveira E, et al. Embryological, clinical and ultrastructural study of human oocytes presenting indented zona pellucida. Zygote. 2015;23:145–57.
13. Ebner T, Moser M, Yaman C, Feichtinger O, Hartl J, Tews G. Elective transfer of embryos selected on the basis of first polar body morphology is associated with increased rates of implantation and pregnancy. Fertil Steril. 1999;72:599–603.
14. Ebner T, Yaman C, Moser M, Sommergruber M, Feichtinger O, Tews G. Prognostic value of first polar body morphology on fertilization rate and embryo quality in intracytoplasmic sperm injection. Hum Reprod. 2000;15:427–30.
15. Cupisti S, Conn CM, Fragouli E, Whalley K, Mills JS, Faed MJW, et al. Sequential FISH analysis of oocytes and polar bodies reveals aneuploidy mechanisms. Prenat Diagn. 2003;23:663–8.
16. Geraedts J, Montag M, Magli MC, Repping S, Handyside A, Staessen C, et al. Polar body array CGH for prediction of the status of the corresponding oocyte. Part I: clinical results. Hum Reprod. 2011;26:3173–80.
17. Schmutzler AG, Acar-Perk B, Weimer J, Salmassi A, Sievers K, Tobler M, et al. Oocyte morphology on day 0 correlates with aneuploidy as detected by polar body biopsy and FISH. Arch Gynecol Obstet. 2014;289:445–50.
18. Zhou W, Fu L, Sha W, Chu D, Li Y. Relationship of polar bodies morphology to embryo quality and pregnancy outcome. Zygote. 2015. doi:10.1017/S0967199415000325.
19. Rienzi L, Ubaldi F, Martinez F, Iacobelli M, Minasi MG, Ferrero S, et al. Relationship between meiotic spindle location with regard to the polar body position and oocyte developmental potential after ICSI. Hum Reprod. 2003;18:1289–93.
20. Petersen CG, Oliveira JBA, Mauri AL, Massaro FC, Baruffi RLR, Pontes A, et al. Relationship between visualization of meiotic spindle in human oocytes and ICSI outcomes: a meta-analysis. Reprod BioMed Online. 2009;18:235–43.
21. Korkmaz C, Tekin YB, Sakinci M, Ercan CM. Effects of maternal ageing on ICSI outcomes and embryo development in relation to oocytes morphological characteristics of birefringent structures. Zygote. 2015;23:550–5.
22. Ménézo Y, Dale B, Cohen M. DNA damage and repair in human oocytes and embryos: a review. Zygote. 2010;18:357–65.
23. Ebner T, Moser M, Yaman C, Sommergruber M, Hartl J, Jesacher K, et al. Prospective hatching of embryos developed from oocytes exhibiting difficult oolemma penetration during ICSI. Hum Reprod. 2002;17:1317–20.
24. Ebner T, Moser M, Sommergruber M, Puchner M, Wiesinger R, Tews G. Developmental competence of oocytes showing increased cytoplasmic viscosity. Hum Reprod. 2003;18:1294–8.
25. Ebner T, Shebl O, Moser M, Sommergruber M, Tews G. Developmental fate of ovoid oocytes. Hum Reprod. 2008;23:62–6.

26. Machtinger R, Politch JA, Hornstein MD, Ginsburg ES, Racowsky C. A giant oocyte in a cohort of retrieved oocytes: does it have any effect on the in vitro fertilization cycle outcome? Fertil Steril. 2011;95:573–6.
27. Sousa M, Barros A, Silva J, Tesarik J. Developmental changes in calcium contents of ultrastructurally distinct subcellular compartments of preimplantation embryos. Mol Hum Reprod. 1997;3:83–90.
28. Wilding M, Dale B, Marino M, di Matteo, Alviggi C, Pisaturo ML, et al. Mitochondrial aggregation patterns and activity in human oocytes and preimplantation embryos. Hum Reprod. 2001;16:909–17.
29. Wells D, Bermúdez MG, Steuerwald N, Malter HE, Thornhill AR, Cohen J. Association of abnormal morphology and altered gene expression in human preimplantation embryos. Fertil Steril. 2005;84:343–55.
30. Gasca S, Pellestor F, Assou S, Loup V, Anahory T, Dechaud H, et al. Identifying new human oocyte marker genes: a microarray approach. Reprod BioMed Online. 2007;14:175–83.
31. Grøndahl ML, Andersen CY, Bogstad J, Nielsen FC, Meinertz H, Borup R. Gene expression profiles of single human mature oocytes in relation to age. Hum Reprod. 2010;25:957–68.
32. Kakourou G, Jaroudi S, Tulay P, Heath C, Serhal P, Haper JC, et al. Investigation of gene expression profiles before and after embryonic genome activation and assessment of functional pathways at the human metaphase II oocyte and blastocyst stage. Fertil Steril. 2013;99:803–14.
33. Alikani M, Palermo G, Adler A, Bertoli M, Blake M, Cohen J. Intracytoplasmic sperm injection in dysmorphic human oocytes. Zygote. 1995;3:283–8.
34. De Sutter P, Dozortsev D, Qian C, Dhont M. Oocyte morphology does not correlate with fertilization rate and embryo quality after intracytoplasmic sperm injection. Hum Reprod. 1996;11:595–7.
35. Sherhal PF, Ranieri DM, Kinis A, Marchant S, Davies M, Khadum IM. Oocyte morphology predicts outcome of intracytoplasmic sperm injection. Hum Reprod. 1997;12:1267–70.
36. Xia P. Intracytoplasmic sperm injection: correlation of oocyte grade based on polar body, perivitelline space and cytoplasmic inclusions with fertilization and embryo quality. Hum Reprod. 1997;12:1750–5.
37. Balaban B, Urman B, Sertac A, Alatas C, Aksoy S, Mercan R. Oocyte morphology does not affect fertilization rate, embryo quality and implantation rate after intracytoplasmic sperm injection. Hum Reprod. 1998;13:3431–3.
38. Loutradis D, Drakakis P, Kallianidis K, Milingos S, Dendrinos S, Michalas S. Oocyte morphology correlates with embryo quality and pregnancy rate after intracytoplasmic sperm injection. Fertil Steril. 1999;72:240–4.
39. Chamayou S, Ragolia C, Alecci C, Storaci G, Maglia E, Russo E, et al. Meiotic spindle presence and oocyte morphology do not predict clinical ICSI outcomes: a study of 967 transferred embryos. Reprod Biomed Online. 2006;13:661–7.
40. Yakin K, Balaban B, Isiklar A, Urman B. Oocyte dysmophism is not associated with aneuploidy in the developing embryo. Fertil Steril. 2007;88:811–6.
41. Figueira RCS, Braga DPAF, Semião-Francisco L, Madaschi C, Iaconelli Jr A, Borges Jr E. Metaphase II human oocyte morphology: contributing factors and effects on fertilization potential and embryo developmental ability in ICSI cycles. Fertil Steril. 2010;94:1115–7.
42. Braga DPAF, Setti AS, Figueira RCS, Machado RB, Iaconelli Jr A, Borges Jr E. Influence of oocyte dysmorphisms on blastocyst formation and quality. Fertil Steril. 2013;100:748–54.
43. Ashrafi M, Karimian L, Eftekhari-Yazdi P, Hasani F, Arabipoor A, Bahmanabadi A, et al. Effect of oocyte dysmorphisms on intracytoplasmic sperm injection cycle outcomes in normal ovarian responders. J Obstet Gynaecol Res. 2015;41:1912–20.
44. Yu EJ, Ahn H, Lee JM, Jee BC, Kim SH. Fertilization and embryo quality of mature oocytes with specific morphological abnormalities. Clin Exp Reprod Med. 2015;42:156–62.
45. Otsuki J, Nagai Y, Chiba K. Lipofuscin bodies in human oocytes as an indicator of oocyte quality. J Assist Reprod Genet. 2007;24:263–70.
46. Kahraman S, Yakin K, Dönmez E, Samli H, Bahçe M, Cengiz G, et al. Relationship between granular cytoplasm of oocytes and pregnancy outcome following intracytoplasmic sperm injection. Hum Reprod. 2000;15:2390–3.
47. Ebner T, Sommergruber M, Moser M, Shebl O, Schreier-Lechner E, Tews G. Basal level of anti-Mullerian hormone is associated with oocyte quality in stimulated cycles. Hum Reprod. 2006;21:2022–6.
48. Ebner T, Moser M, Sommergruber M, Gaiswinkler U, Shebl O, Jesacher K, et al. Occurrence and developmental consequences of vacuoles throughout preimplantation development. Fertil Steril. 2005;83:1635–40.
49. Bianchi V, Macchiarelli G, Borini A, Lappi M, Cecconi S, Miglietta S, et al. Fine morphological assessment of quality of human mature oocytes after slow freezing or vitrification with a closed device: a comparative analysis. Reprod Biol Endocrinol. 2014;12:110. doi: 10.1186/1477-7827-12-110.
50. Palmerini MG, Antinori M, Maione M, Cerusico F, Versaci C, Nottola SA, et al. Ultrastructure of immature and mature human oocytes after cryotop vitrification. J Reprod Dev. 2014;60:411–20.
51. Bianchi S, Macchiarelli G, Micara G, Linari A, Boninsegna C, Aragona C, et al. Ultrastructural markers of quality are impaired in human metaphase II aged oocytes: a comparison between reproductive and in vitro aging. J Assist Reprod Genet. 2015;32:1343–58.
52. Fancsovits P, Murber A, Gilán ZT, Rigó Jr J, Urbancsek J. Human oocytes containing large cytoplasmic vacuoles can result in pregnancy and viable offspring. Reprod BioMed Online. 2011;23:513–6.
53. Otsuki J, Okada A, Morimoto K, Nagai Y, Kubo H. The relationship between pregnancy outcome and smooth endoplasmic reticulum clusters in MII human oocytes. Hum Reprod. 2004;19:1591–7.
54. Ebner T, Moser M, Shebl O, Sommerguber M, Tews G. Prognosis of oocytes showing aggregation of smooth endoplasmic reticulum. Reprod BioMed Online. 2008;16:113–8.
55. Akarsu C, Çağlar G, Vicdan K, Sözen E, Biberoğlu K. Smooth endoplasmic reticulum aggregations in all retrieved oocytes causing recurrent multiple anomalies: case report. Fertil Steril. 2009;92(1496):e1–3.
56. Sá R, Cunha M, Silva J, Luís A, Oliveira C, Teixeira da Silva J, et al. Ultrastructure of tubular smooth endoplasmic reticulum aggregates in human metaphase II oocytes and clinical implications. Fertil Steril. 2011;96:143–9.
57. Mateizel I, Van Landuyt L, Tournaye H, Verheyen G. Deliveries of normal healthy babies from embryos originating from oocytes showing the presence of smooth endoplasmic reticulum aggregates. Hum Reprod. 2013;28:2111–7.
58. Hattori H, Nakamura Y, Nakajo Y, Araki Y, Kyono K. Deliveries of babies with normal health derived from oocytes with smooth endoplasmic reticulum clusters. J Assist Reprod Genet. 2014;31:1461–7.
59. Shaw-Jackson C, Van Beirs N, Thomas A-L, Rozenberg S, Autin C. Can healthy babies originate from oocytes with smooth endoplasmic reticulum aggregates? A systematic mini-review. Hum Reprod. 2014;29:1380–6.
60. Restelli L, Noci SD, Mangiarini A, Ferrari S, Somigliana E, Paffoni A. The impact of Alpha/ESHRE consensus regarding oocytes with aggregates of smooth endoplasmic reticulum (SERa) on in vitro fertilization outcome. J Assist Reprod Genet. 2015;32:1629–35.
61. Van Beirs N, Shaw-Jackson C, Rozenberg S, Autin C. Policy of IVF centres towards oocytes affected by smooth endoplasmic reticulum aggregates: a multicentric survey study. J Assist Reprod Genet. 2015;32:945–50.
62. Rooney DE, Czepulkowski BH. Human chromosome preparation. Essential techniques. UK: John Wiley & Sons Ltd; 1997 (Series Editor: B Rickwood).
63. Huirne JA, Homburg R, Lambalk CB. Are GnRH antagonists comparable to agonists for use in IVF? Hum Reprod. 2007;22:2805–13.

64. Pinto F, Oliveira C, Cardoso MF, Teixeira da Silva J, Silva J, Sousa M, et al. Impact of GnRH ovarian stimulation protocols on intracytoplasmic sperm injection outcomes. Reprod Biol Endocrinol. 2009;7:5. doi:10.1186/1477-7827-7-5.
65. Tesarik J, Sousa M. Key elements of a highly efficient intracytoplasmic sperm injection technique: Ca^{2+} fluxes and oocyte cytoplasmic dislocation. Fertil Steril. 1995;64:770–6.
66. Vandervorst M, Liebaers I, Sermon K, Staessen C, De Vos A, Van de Velde H, et al. Successful preimplantation genetic diagnosis is related to the number of available cumulus-oocyte complexes. Hum Reprod. 1998;13:3169–76.
67. Gardner DK, Lane ML, Stevens J, Schlenker T, Schollcraft WB. Blastocyst score affects implantation and pregnancy outcome: towards a single blastocyst transfer. Fertil Steril. 2000;73:1155–8.
68. Radesic B, Tremellen K. Oocyte maturation employing a GnRH agonist in combination with low-dose hCG luteal rescue minimizes the severity of ovarian hyperstimulation syndrome while maintaining excellent pregnancy rates. Hum Reprod. 2011;26:3437–42.
69. Sousa M, Tesarik J. Ultrastructural analysis of fertilization failure after intracytoplasmic sperm injection. Hum Reprod. 1994;9:2374–80.
70. El Shafie M, Sousa M, Windt M-L, Kruger TF. An atlas of the ultrastructure of human oocytes. A guide for assisted reproduction. NY, USA: The Parthenon Publishing Group; 2000.
71. Coonen E, Dumoulin JCM, Ramaekers FCS, Hopman AHN. Optimal preparation of preimplantation embryo interphase nuclei for analysis by fluorescence in-situ hybridization. Hum Reprod. 1994;9:533–7.
72. Harper JC, Coonen E, Ramaekers FCS, Delhanty JDA, Handyside AH, Wilston RML, et al. Identification of the sex of human preimplantation embryos in two hours using an improved spreading method and fluorescent in-situ hybridization (FISH) using directly labelled probes. Hum Reprod. 1994;9:721–4.
73. Alves C, Sousa M, Silva J, Barros A. Preimplantation genetic diagnosis using FISH for carriers of Robertsonian translocations: the Portuguese experience. Prenat Diagn. 2002;22:1153–62.
74. Turnpenny P, Ellard S. Emery's elements of medical genetics. Philadelphia, USA: Elsevier, Churchill Livingstone; 2012.
75. Forabosco A, Percesepe A, Santucci S. Incidence of non-age-dependent chromosomal abnormalities: a population-based study on 88965 amniocenteses. Eur J Hum Genet. 2009;17:897–903.
76. Papanikolaou EG, Vernaeve V, Kolibianakis E, Van Assche E, Bonduelle M, Liebaers I, et al. Is chromosome analysis mandatory in the initial investigation of normovulatory women seeking infertility treatment? Hum Reprod. 2005;20:2899–903.
77. Shevell T, Malone FD, Vidaver J, Porter TF, Luthy DA, Comstock CH, et al. Assisted reproductive technology and pregnancy outcome. Obstet Gynecol. 2005;106:1039–45.
78. Ravel C, Berthaut I, Bresson JL, Siffroi JP, et al. Prevalence of chromosomal abnormalities in phenotypically normal and fertile adult males: large-scale survey of over 10000 sperm donor karyotypes. Hum Reprod. 2006;21:1484–89.
79. Clementini E, Palka C, Iezzi L, Stuppia L, Guanciali-Franchi P, Tiboni GM. Prevalence of chromosomal abnormalities in 2078 infertile couples referred for assisted reproductive techniques. Hum Reprod. 2005;20:437–42.
80. Ferlin A, Raicu F, Gatta V, Zuccarello D, Palka G, Foresta C. Male infertility: role of genetic background. Reprod BioMed Online. 2007;14:734–45.
81. Gekas J, Thepot F, Turleau C, Siffroi JP, Dadoune JP, Wasels R, et al. Chromosomal factors of infertility in candidate couples for ICSI: an equal risk of constitutional aberrations in women and men. Hum Reprod. 2001;16:82–90.
82. Schreurs A, Legius E, Meuleman C, Fryns J-P, D'Hooghe TM. Increased frequency of chromosomal abnormalities in female partners of couples undergoing in vitro fertilization or intracytoplasmic sperm injection. Fertile Steril. 2000;74:94–6.
83. De Sutter P, Stadhoufers R, Dutré M, Gerris J, Dhont M. Prevalence of chromosomal abnormalities and timing of karyotype analysis in patients with recurrent implantation failure (RIF) following assisted reproduction. FVV ObGyn. 2012;4:59–65.
84. Sousa M, Barros A, Tesarik J. Developmental changes in calcium dynamics, protein kinase C distributions and endoplasmic reticulum organization in human preimplantation embryos. Mol Hum Reprod. 1996;2:967–77.
85. Norppa H, Falck GC-M. What do human micronuclei contain? Mutagenesis. 2003;18:221–33.
86. Shimizu N. Molecular mechanisms of the origin of micronuclei from extrachromosomal elements. Mutagenesis. 2011;26:119–23.
87. Mantikou E, Wong KM, Repping S, Masteenbroek S. Molecular origin of mitotic aneuploidies in preimplantation embryos. Biochem Biophy Acta. 1822;2012:1921–30.
88. Nottola SA, Macchiarelli G, Familiari G. Fine structural markers of human oocyte quality in assisted reproduction. Austin J Reprod Med Infertil. 2014;1:5.